Geoscience Frontiers 14 (2023) 101619

HOSTED BY

Contents lists available at ScienceDirect

Geoscience Frontiers

journal homepage: www.elsevier.com/locate/gsf

Research Paper

An updating of landslide susceptibility prediction from the perspective of space and time

Zhilu Chang [a,b], Faming Huang [a,*], Jinsong Huang [a,d], Shui-Hua Jiang [a], Yuting Liu [c], Sansar Raj Meena [b], Filippo Catani [b]

[a] School of Infrastructure Engineering, Nanchang University, Nanchang 330031, China
[b] Department of Geosciences, University of Padua, Padua, Italy
[c] Department of Civil, Environmental and Architectural Engineering, University of Padua, Padova, Italy
[d] Discipline of Civil, Surveying and Environmental Engineering, Priority Research Centre for Geotechnical Science and Engineering, University of Newcastle, NSW, Australia

ARTICLE INFO

Article history:
Received 14 November 2022
Revised 14 March 2023
Accepted 14 April 2023
Available online 20 April 2023
Handling Editor: Wengang Zhang

Keywords:
Landslide susceptibility updating
Spatial effect
Temporal effect
Machine learning

ABSTRACT

Due to the similarity of conditioning factors, the aggregation feature of landslides and the multi-temporal landslide inventory, the spatial and temporal effects of landslides need to be considered in landslide susceptibility prediction (LSP). The ignorance of this issue will result in some biases and time-invariance in landslide susceptibility. Hence, a novel framework has been proposed to update landslide susceptibility by simultaneously considering the spatial and temporal effects of landslides at the regional scale. In this framework, the landslide inventory of Chongyi County has been divided into pre- and fresh-landslide inventories. According to the LSP results predicted by the support vector machine (SVM) model using the slope unit-based conditioning factors and pre-landslide inventory, a normalized spatial distance index (NSDI) is calculated to quantitatively represent the spatial correlation between landslides and surrounding slope units to develop the SVM-NSDI model. Furthermore, the SVM-Updating model, which incorporates the LSP results of the SVM-NSDI model and fresh-landslide inventory, could be developed to update the LSP results. Subsequently, the confusion matrix, the area under the receiver operating characteristic curve (AUC) and frequency ratio (FR) accuracy are used to evaluate the prediction performance of the above LSP models. The F_1-score values of the SVM, SVM-NSDI and SVM-Updating models are 0.776, 0.816 and 0.831, respectively. The AUC values are 0.869, 0.903 and 0.914 and the FR accuracies are 0.795, 0.853 and 0.873. It can be concluded that landslide susceptibility is a time-variant variable, which can be updated by considering the spatial correlation between landslides and surrounding slope units as well as the temporal effects of multi-temporal landslide inventory. This study provides a new framework to update landslide susceptibility over time and also provides more accurate LSP results for decision-makers.

1. Introduction

Landslide susceptibility prediction (LSP) has been an effective technique to predict the spatial distribution of landslides that are likely to occur at the regional scale, by calculating the likelihood of a landslide occurring based on the topographical, geological, hydrological, land cover and other conditioning factors as well as the recorded landslide information (Reichenbach et al., 2018; Liu et al., 2023). Recently, lots of studies of LSP focus on the mapping unit extraction, conditioning factors selection, comparison of different LSP models, uncertainty analysis in landslide susceptibility modeling and other aspects to promote the application of LSP for landslide risk assessment and prevention (Merghadi et al., 2020; Huang et al., 2021a,2021b; Zhou et al., 2021; Yang et al., 2022; Chang et al., 2023). In those studies, however, the landslide susceptibility is normally thought of as a time-invariant concept, which means that it remains constant throughout time for a given location, the spatial and temporal effects of landslides have been neglected in the LSP process. Moreover, if the temporal effect is considered in landslide susceptibility, it will fall under the purview of landslide hazards (Guzzetti et al., 1999; Al-Najjar and Pradhan, 2021).

* Corresponding author.
E-mail address: faminghuang@ncu.edu.cn (F. Huang).

https://doi.org/10.1016/j.gsf.2023.101619

Conversely, a new concept of time-variant landslide susceptibility or dynamic landslide susceptibility has been proposed by Samia et al. (2020), which means that the landslide susceptibility of a place changes over time. Several evidence could be provided to support on this concept. First, subsequent landslides are more likely to occur with a wider and rounder scope over a period of about 10 years as a result of the clear legacy effect of earlier landslides (Phillips, 2006; Parker et al., 2015; Temme et al., 2015; Samia et al., 2017a). Then, the observations indicate that fresh landslides are more likely to occur when they are situated close to the center of a previous landslide in space (Fan et al., 2015; Samia et al., 2017b). Apparently, the landslide susceptibility would change over time as more valuable information could be provided by the multi-temporal inventory in a region (Tseng et al., 2015). Moreover, some literature also shows that the spatial and temporal probabilities of landslides are not independent (Guzzetti et al., 2005). Furthermore, time-related internal conditioning factors also play an important role in determining the landslide susceptibility (Singh et al., 2014; Samia et al., 2017a). Therefore, since the time-variant property of landslide susceptibility exists, the effects of fresh landslides on landslide susceptibility should be taken into account and quantified to update the landslide susceptibility.

Although landslide susceptibility has been deeply studied with many encouraging results based on a wide range of statistical and machine learning techniques (Youssef et al., 2015; Ji et al., 2022; Zhou et al., 2022; Zhang et al., 2023), only few studies taken the time-variant property into account to update landslide susceptibility from the following perspectives: First, the intuitive and simple method is to continually integrate the information of fresh landslides with the previous landslide inventory as the multi-temporal landslide inventory to predict landslide susceptibility (Guzzetti et al., 2012; Del Ventisette et al., 2014). However, the drawbacks of operation difficulty, consumption of time and labor temporarily limit the updating of multi-temporal landslide inventories with sufficient resolution in time. Additionally, the updating performance is unsatisfactory when the number of fresh landslides is lower. Focusing on the multi-temporal landslide inventories, Samia et al. (2018, 2020) have implemented the transient effects of earlier landslides on the susceptibility of further landslides in a promising perspective by using "landslide path dependency". The path dependency has been characterized and quantified by a space–time clustering measure. Two landslide path dependency variables are applied to describe the transient effects on landslide susceptibility based on the multi-temporal landslide inventories from the Collazzone area in Italy. However, the essential limitation of this method is that the landslide inventories in most areas are not multi-temporal due to the difficulty of obtaining high-resolution multi-temporal datasets, resulting in the restricted application.

According to the other perspective, the landslide susceptibility can be updated using the Bayes method by respectively regarding the pre- and fresh-landslide inventory information as the prior and posterior information based on the physically-based models (Wang et al., 2019; Depina et al., 2020). Although the physical mechanism of landslides has been considered in physically-based models and the Bayesian updating theory has been widely applied in geotechnical engineering (Jiang et al., 2018; Wang et al., 2020). It is difficult to collect geotechnical and hydrological data in detail on a large scale, resulting in low accuracy and difficulty in application promotion of this method. Hence, this method can only be implemented on a small scale or on a single slope. Above all, how to quantify the effect of fresh landslide on landslide susceptibility is still an important issue that needs to be solved urgently.

In the previous landslide susceptibility updating literature, another critical and frequently neglected issue is that the spatial correlation between the landslides and their surrounding zones has not been quantified. It is illustrated that the spatial distribution of landslides on a regional scale shows the aggregation feature in actual practice (Wang et al., 2013; Liu et al., 2019), which can be explained by the fact that natural clustering is a common phenomenon. In addition, some conditioning factors (such as geological strata, topography, hydrology, soil properties, etc.) that control landslide occurrence have similar characteristics with strong spatial correlation in a specific area. The ignorance of spatial correlation will lead to some biases about the susceptibility of follow-up landslides. Fortunately, the Euclidean distance is an effective and widely used indicator in spatial correlation analysis for quantitatively quantifying the correlation between two points in space (Liu et al., 2019; Gojcic et al., 2021). Hence, it provides a new perspective to achieve the landslide susceptibility updating by taking the spatial correlation between fresh landslides and the surrounding area into account.

Aiming at the aforementioned issues, the main objective of this study is to update the landslide susceptibility from the perspective of space and time. In the space perspective, the spatial correlation between landslides and surrounding slope units within a certain distance has been quantified by the Euclid distance and a normalized spatial distance index (NSDI). In the time perspective, the landslide inventory is divided into pre- and fresh-landslide inventories. The pre-landslide inventory is used to predict landslide susceptibility and the fresh-landslide inventory is applied to update landslide susceptibility. This method is illustrated and validated using an example in Chongyi County, China.

2. Method

2.1. Procedure of landslide susceptibility updating

The flowchart of landslide susceptibility updating is shown in Fig. 1. The main procedures of this method include:

(1) Preparation of basic data and landslide inventory: the basic topographic, geological, hydrological and land cover data of the study area are collected. The landslide inventory is constructed by field investigation and historical information collection, which is classified into pre-landslide inventory (1970–2005) and fresh-landslide inventory (2006–2019). In addition, slope units are extracted by the multi-scale segmentation method as the basic mapping unit.

(2) Development of a slope unit-based SVM model and calculation of landslide susceptibility indexes: some slope unit-based conditioning factors, including topographic, geological, hydrological, land cover and others, are extracted as the basic input data. The SVM model is applied to develop a slope unit-based SVM model and calculate the landslide susceptibility indexes, which can be divided into five landslide susceptibility levels (very low, low, moderate, high and very high).

(3) Development of SVM-NSDI model considering the spatial correlation between landslides and slope units: In this process, the Euclidean distance is calculated to represent the spatial correlation between landslide points and surrounding slope unit points. For each slope unit with a very high landslide susceptibility level, the distance that is closest to a landslide is chosen. As a result, the maximum value of those closest distances is determined as the distance threshold (Dt) between landslides and the slope units with very high landslide susceptibility level. Then, the value of NSDI is calculated to develop the SVM-NSDI model and calculate the landslide susceptibility indexes considering the spatial correlation between landslides and slope units, which can

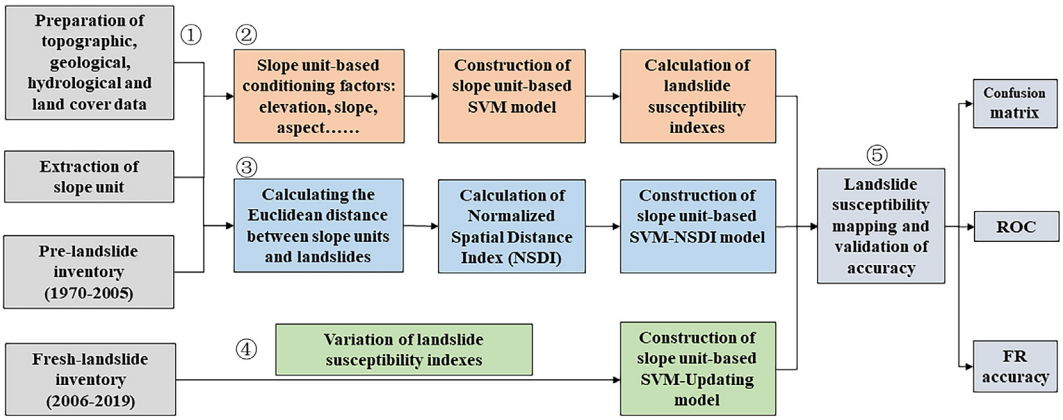

Fig. 1. The flowchart of landslide susceptibility updating.

be considered as the prior landslide susceptibility information.

(4) Construction of the SVM-Updating model: the distances between each fresh landslide and slope units within Dt are calculated. Then the NSDI between fresh landslides and slope units can be calculated. For the slope unit that occurred fresh landslide, the LSP value is up to 1, and the variation of LSP values can be calculated. Furthermore, the LSP variation of other slope units can be calculated by multiplying the sum of NSDI and the LSP variation value of slope units with fresh landslides. As a result, the SVM-Updating model can be developed to update the LSP values by adding the LSP variation and the LSP values of SVM-NSDI model.

(5) Landslide susceptibility mapping and accuracy validation: based on the LSP results of SVM, SVM-NSDI and SVM-Updating models, the landslide susceptibility indexes of those models are classified into five levels to obtain the landslide susceptibility mapping. In addition, confusion matrix, the receiver operating characteristic (ROC) curve and frequency ratio (FR) accuracy are used to validate the performance of those models.

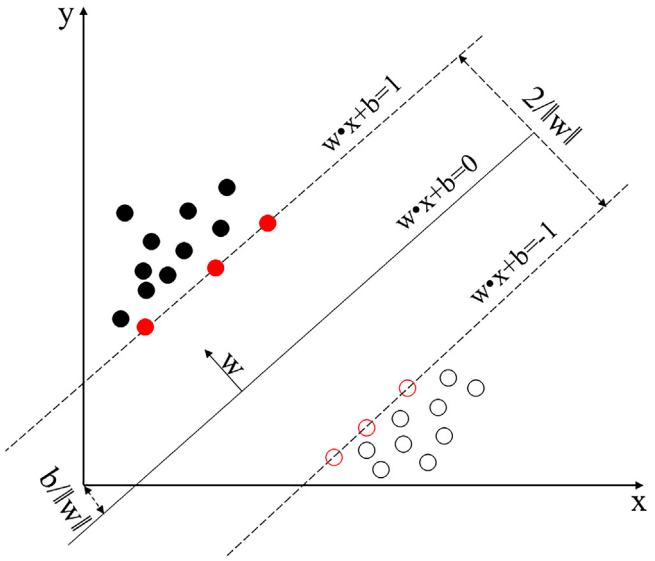

Fig. 2. The schematic diagram of SVM model.

2.2. Support vector machine model

Currently, some machine learning models have been commonly used to predict landslide susceptibility, hazard and risk with better performances than traditional statistical methods (Reichenbach et al., 2018). The SVM model is selected as the basic machine learning model to predict landslide susceptibility due to its higher accuracy than other machine learning models. Meanwhile, it is also an effective supervised machine learning model to solve non-linear binary classification problems (Merghadi et al., 2020). The goal of this method is to convert the original input data into a higher-dimensional feature space to maximally split input data into two classes by finding the best n-dimensional hyper-plane.

The schematic diagram of SVM model is shown in Fig. 2. Suppose a training dataset in a feature space: $T = \{(x_1, y_1), (x_2, y_2), \ldots, (x_n, y_n)\}$, the x_i ($i = 1, 2, \ldots, n$) is a series of input variables and the $y_i \in \{-1, +1\}, i = 1, 2, \ldots, n$ corresponds to output of binary-classification. For the hyper-plane of $w \cdot x + b = 0$, the classification margin of this hyper-plane and sample points (x_i, y_i) can be calculated by Eq. (1). The minimum of classification margin is represented by Eq. (2).

$$\gamma_i = y_i\left(\frac{w}{\|w\|}\cdot x_i + \frac{b}{\|w\|}\right) \tag{1}$$

$$\gamma = \min_{i=1,2,\ldots,n} \gamma_i \tag{2}$$

The maximum separating hyper-plane solution of SVM model can be expressed as the following constrained optimization problem:

$$\frac{1}{2}\| w \|^2 \tag{3}$$

$$y_i(\omega \cdot x_i) + b \geq 1 \tag{4}$$

where $\| w \|^2$ is the norm of the normal of the hyper-plane, b is regarded to be a constant value. The Lagrangian forma is used to define the cost function as:

$$L = \| w \|^2/2 - \sum_{i=1}^{N} \lambda_i((y_i(\omega \cdot x_i) + b) - 1) \tag{5}$$

where λ_i is the Lagrange multiplier. The radial basis function is selected in this study as Eq. (6), where δ represents the gamma term of the kernel function:

$$K(x_i, y_j) = \exp(-\delta\| x_i - x_j \|^2), \ \delta > 0 \tag{6}$$

2.3. Normalized spatial distance index

According to the similar characteristics of conditioning factors and the aggregation feature of landslides in actual practice (Liu et al., 2019), the spatial correlation between landslide points and slope unit points has been taken into account by Euclidean distance (Gojcic et al., 2021). The landslide and slope unit points are determined by the centroids of landslide and slope unit polygons. For each landslide point, based on the Euclidean distance within the distance of Dt, the NSDI is used to quantitatively represent the effect of each landslide on its surrounding slope units, which can be calculated using the Eq. (7):

$$\mathrm{NSDI}_{i,j} = \frac{\mathrm{Max}(d_{L_i,S_j}) - d_{L_i,S_j}}{\mathrm{Max}(d_{L_i,S_j}) - \mathrm{Min}(d_{L_i,S_j})} \ (i = 1,2,\ldots,m;\ j = 1,2,\ldots,n) \quad (7)$$

where the L_i represents the number of landslides, the S_j represents the number of slope units, the d_{L_i,S_j} represents the Euclidean distance between landslide of L_i and slope unit of S_j, the $\mathrm{Max}(d_{L_i,S_j})$, $\mathrm{Min}(d_{L_i,S_j})$ respectively represents the maximum and minimum value of d_{L_i,S_j}.

2.4. A conceptual example of landslide susceptibility updating

To visualize the process of landslide susceptibility updating in Fig. 1, a conceptual example has been shown in Fig. 3. There are a total of 16 slope units (S_1, S_2, …, S_{16}) and the landslide susceptibility levels of those slope units have been predicted using machine learning models, which can be used as the prior landslide susceptibility information (Fig. 3a). Then suppose two fresh landslides (L_1, L_2) have respectively occurred in slope units of S_7 and S_{15} (Fig. 3b), and suppose the landslide susceptibility indexes of S_7 and S_{15} have increased to 1. For the landslide of L_1 (or L_2), the Euclidean distances between L_1 (or L_2) and their surrounding slope units ($d_{Li,Sj}$) are calculated (Fig. 3c). Next, the NSDI value, represented by $q^{Li,Sj}$, can be calculated using Eq. (7) (Fig. 3d). For each slope unit, the total effect induced by its surrounding landslides can be obtained by adding the NSDI values of the surrounding landslides (Fig. 3e), For the S_{10}, the total effect induced by its surrounding landslides can be obtained by $q^{S10} = q^{L1,S10} + q^{L2,S10}$. Lastly, the landslide susceptibility level for each slope unit can be updated by integrating the spatial effect of fresh landslides on surrounding slope units and the landslide susceptibility variation of slope units where fresh landslides occurred (Fig. 3f). For example, the landslide susceptibility levels of S_2, S_3, S_9, S_{10} and S_{11} have been updated from high, low, high, moderate and high levels to very high, high, very high, very high and very high levels.

2.5. Model evaluation

The confusion matrix-based statistical indices, the ROC curve and the FR accuracy are widely utilized to evaluate and compare the prediction performance of different LSP models (Ng et al., 2021; Wang et al., 2021). In the confusion matrix, true positive (*TP*) is the positive sample that is predicted as positive, false positive (*FP*) is the negative sample that is predicted as positive, true negative (*TN*) is the negative sample that is predicted as negative, false negative (*FN*) is the positive sample that is predicted as negative. The precision is defined as the ratio *TP* to (*TP* + *FP*), and the recall is defined as the ratio *TP* to (*TP* + *FN*). The accuracy, and F_1-score can be calculated by Eqs. (8) and (9). The ROC curve is drawn by setting false positive rate (1-specificity) and true positive rate (sensitivity) as the horizontal as well as vertical axes based on the confusion matrix. The FR accuracy is calculated through dividing the sum FR value of very high and high landslide susceptibility levels by the sum FR value of all landslide susceptibility levels. More details about the ROC curve and the FR accuracy can be found in the literature of Huang et al. (2022).

$$Accuracy = \frac{TP + TN}{TP + FP + TN + FN} \quad (8)$$

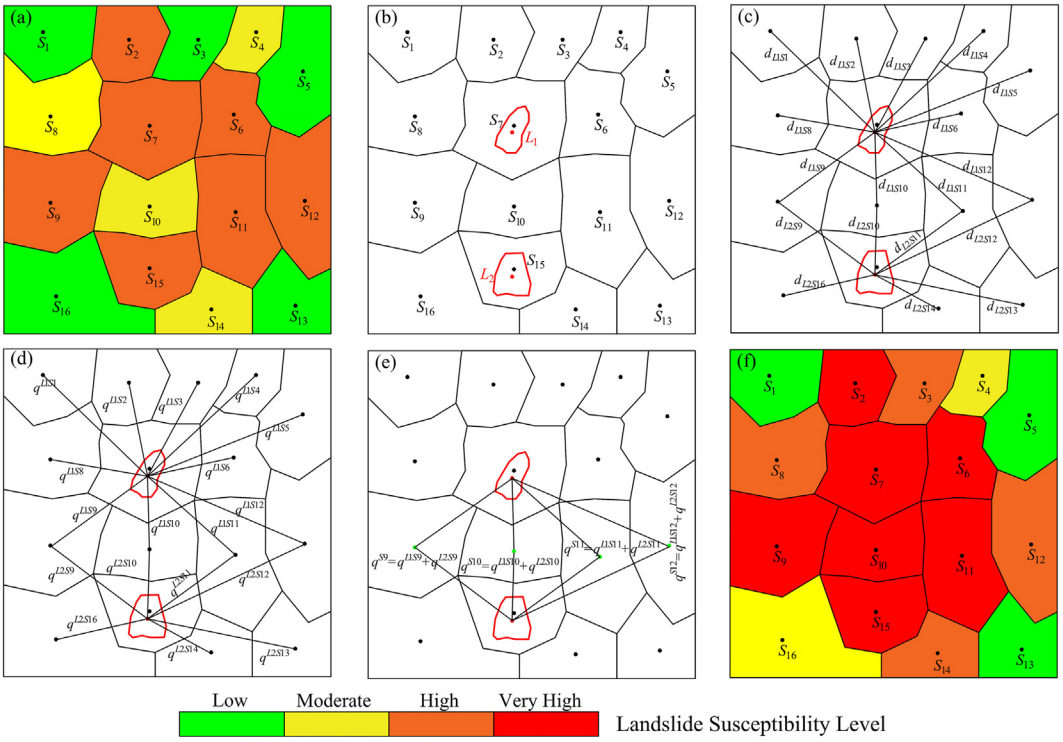

Fig. 3. A conceptual example of landslide susceptibility updating.

$$F_1 - score = \frac{2 \times Precision \times Recall}{Precision + Recall} \quad (9)$$

3. Case study

3.1. Introduction of Chongyi County

Chongyi County, shown in Fig. 4a, is selected as a suitable study case. The site lies between the latitudes 25°24′N–25°55′N and longitudes 113°55′E–114°38′E. It covers an area of approximately 2,206.27 km^2. In this study area, the elevation ranges from 142 to 1998 m. The climate belongs to a sub-tropical monsoon climate, and the annual average rainfall is up to 1615 mm. The initial landslide inventory of 235 landslides has been constructed based on remote sensing interpretation and field survey results in 2005. Since then, a total of 16 landslides have been collected from 2006 to 2019. Because the occurrence time of some landslides is unknown and the number of landslides (2006–2019) is small, the landslide inventory is classified into pre-landslide inventory (1970–2005) and fresh-landslide inventory (2006–2019) to respectively predict and update landslide susceptibility.

The distribution of pre-landslide (red points) and fresh-landslide (green points) inventories are shown in Fig. 4b. These landslides can be regarded as shallow landslides with the characteristic of small scale and group occurrence. The landslide area ranges from 4.2 × 10^2 to 9.2 × 10^4 m^2 with the average value of 2.5 × 10^4 m^2. The thicknesses of landslides vary between 2.8 and 8.0 m. Furthermore, the main triggering factors of landslides occurrence are seasonal heavy rainfall and human activities. Especially with the construction of roads in the mountains, lots of landslides have occurred on the sides of road slopes under the heavy rainfall conditions. For example, two typical landslides are shown in Fig. 4-c-d. This is because that the stress condition and stability of the slope have been changed by the slope cutting, and the overburden soils of the slope are prone to occur landslides in a small area with heavy rainfall, resulting in traffic disruption and a threat to vehicles and pedestrians.

3.2. Selection and FR analysis of conditioning factors

Landslides are usually induced by the combined effects of topographic, geological, hydrological, human activity and land cover conditioning factors. Those conditioning factors are used to develop LSP models as the basic input variables when using the statistical method. Some literature has listed and suggested a series of conditioning factors for LSP (Huabin et al., 2016; Reichenbach et al., 2018; Yong et al., 2022). However, not all conditioning factors can contribute to LSP and have positive influences. Moreover, the same conditioning factor affects LSP differently depending on the locale and landslide type. According to the suggested conditioning factors in the literature, the correlation analysis method has been used to select suitable conditioning factors. Some conditioning factors that have a strong correlation (correlation coefficient larger than 0.30) will be removed. Consequently, 12 conditioning factors, including elevation, slope, aspect, profile curvature, plan curvature, relief amplitude, lithology, topographic wetness index, normalized difference built-up index (NDBI), nor-

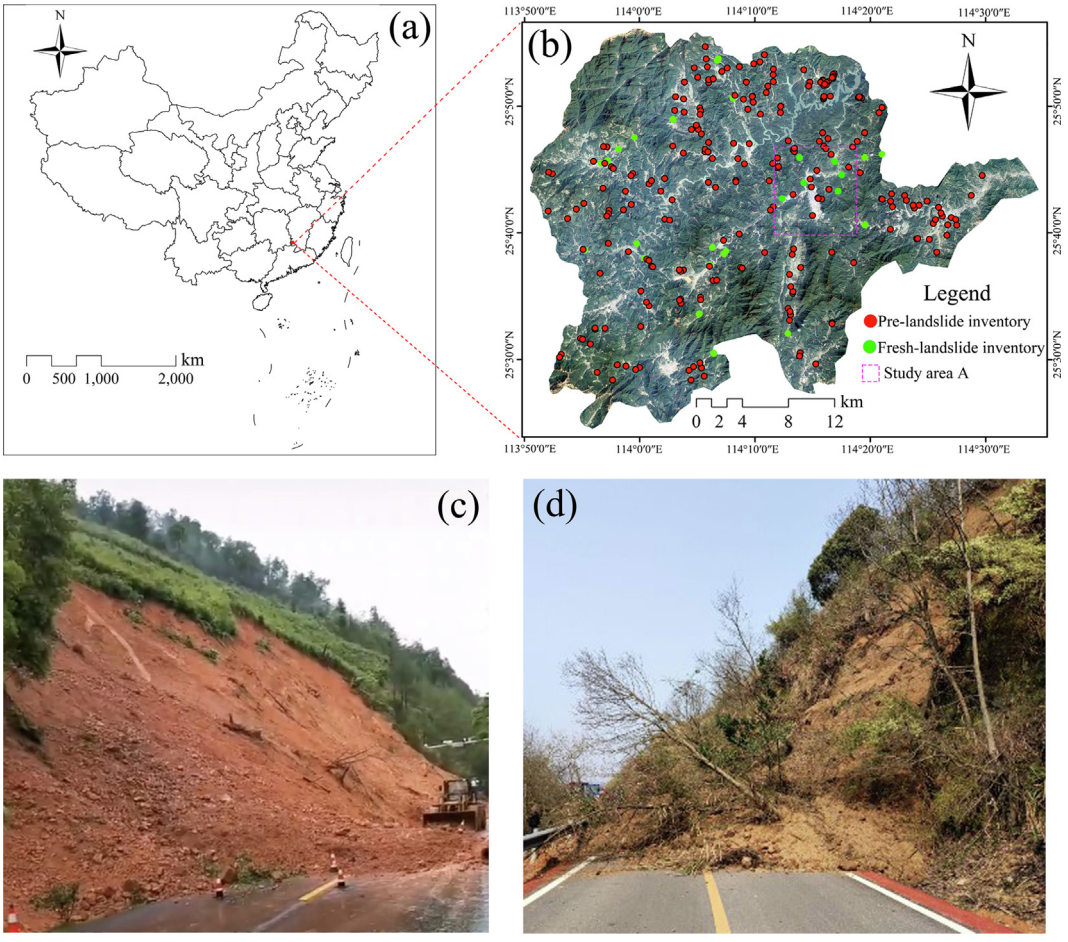

Fig. 4. The location and historical landslide inventory map of Chongyi County.

malized difference vegetation index (NDVI), river density and road density, are extracted using ArcGIS 10.2 software.

In this study, the slope unit is used as the basic mapping unit, which can be automatically extracted by the multi-scale segmentation method proposed by Huang et al. (2021a). There are a total of 53,055 slope units in this study area. Based on the pixel-based conditioning factor maps with a resolution of 8.9 m, the slope unit-based conditioning factors can be extracted using the zoning statistical function in the ArcGIS 10.2 software. The slope unit-based conditioning factor maps are shown in Fig. 5. Afterwards, to reduce the effect of different dimensions or scales of conditioning factors on LSP, the FR method has been used to unify and construct the relationship between landslides and conditioning factors (Chang et al., 2020). In this method, it is important to determine the attribution numbers of each conditioning factor in landslide susceptibility modeling. There is no uniform standard for dividing the attribution numbers of conditioning factors. Huang et al. (2021b) have explored the influences of different attribution numbers of conditioning factors on the uncertainties of LSP. Hence, based on the studies of Huang et al. (2021b), the attribution numbers of continuous slope unit-based conditioning factors are determined to be 8 using the natural break point method in ArcGIS software. For the discrete slope unit-based conditioning factors, the attribution numbers are determined according to the number of types contained in the conditioning factor. For example, the lithology is divided by strata configuration and the aspect is divided into 9 classes. The FR results of conditioning factors are summarized in Table 1. For each class of conditioning factors, the larger the FR value is, the greater the contribution to landslide is. For example, the FR values of 142 m–311 m, 311 m–421 m are larger than 1, representing that the area between 142 m and 421 m is prone to occur landslides.

3.3. Preparation of the sample datasets and development of models

It is indispensable to prepare a dataset including conditioning factors and labeled data for machine learning model development. Then the dataset is divided into training and testing dataset with a predetermined ratio. The training dataset is generally applied for building LSP models, and the testing dataset is used to validate the prediction performance of LSP models (Hong et al., 2019; Sun et al., 2022). The labeled data consists of landslide data with a

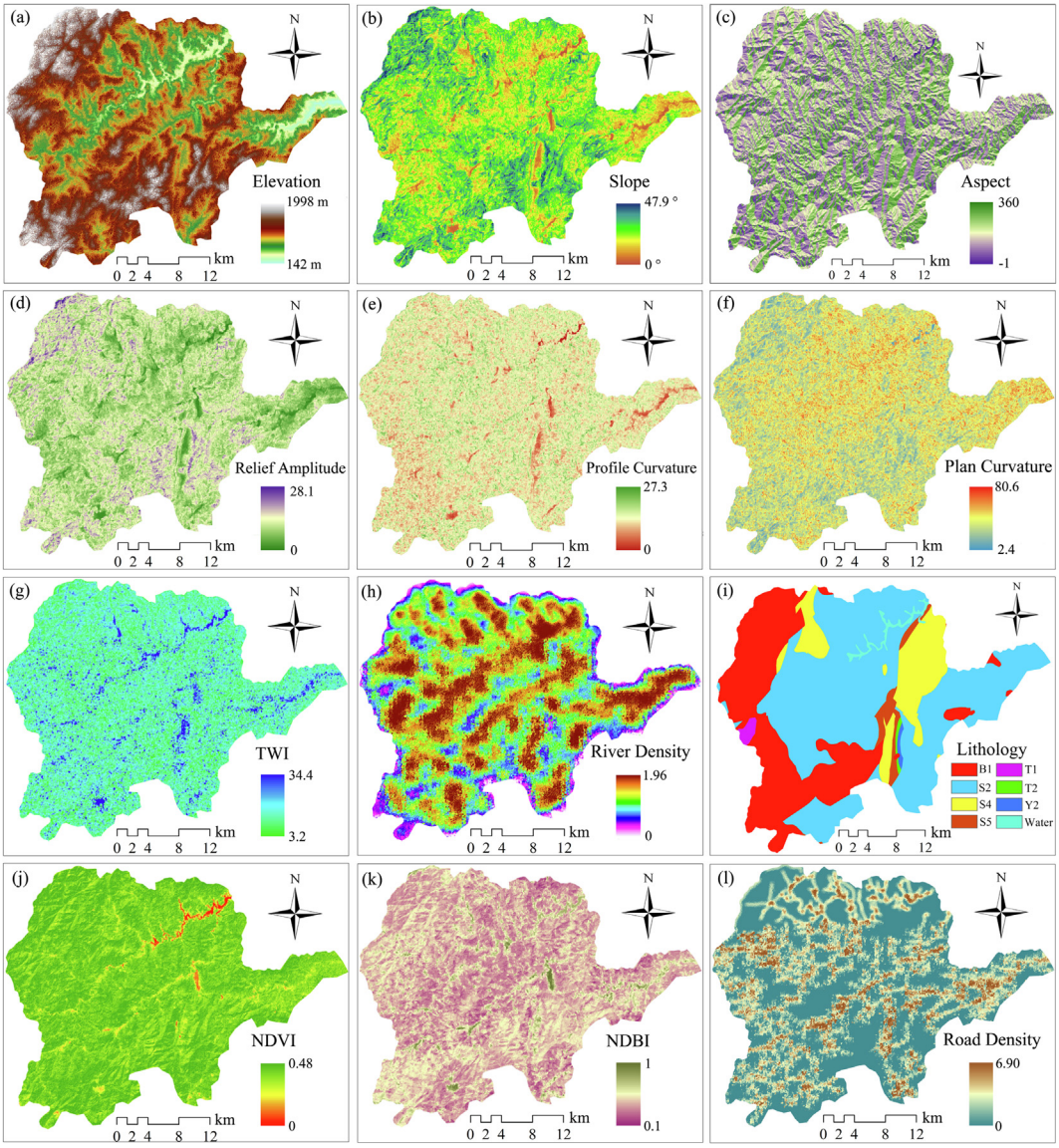

Fig. 5. Slope unit-based conditioning factors in Chongyi County.

Table 1
The data source, classification and FR values of conditioning factors.

Conditioning factors	Source	Spatial resolution	Classification standard and FR values
DEM (m)	ASTER satellite	8.9 m	[142, 311, 2.409]; (311, 421, 1.078]; (421, 536, 0.797]; (536, 669, 0.646]; (669, 823, 0.527]; (823, 996, 0.36]; (996, 1234, 0.162]; (1234, 1998, 0]
Slope (°)	DEM	8.9 m	[0, 6.38, 1.674]; (6.38,10.5, 1.794]; (10.5, 13.88, 0.999]; (13.88, 17.09, 0.916]; (17.09, 20.4, 0.775]; (20.4,24.19, 0.717]; (24.19, 29.07, 0.2]; (29.07, 47.88, 0.099]
Aspect (°)	DEM	8.9 m	[0, 22.5, 0.437]; (22.5, 67.5, 0.906]; (67.5, 112.5, 1.155]; (112.5,157.5, 0.829]; (157.5, 202.5, 0.917]; (202.5, 247.5, 1.301]; (247.5, 292.5, 1.171]; (292.5, 337.5, 0.973]; (337.5, 360, 0.437]
Profile curvature	DEM	8.9 m	[0, 3.37, 1.27]; (3.37, 5.07, 1.395]; (5.07, 6.41, 1.201]; (6.41, 7.72, 1.154]; (7.72, 9.19, 0.804]; (9.19, 11.06, 0.763]; (11.06, 13.85, 0.432]; (13.85, 27.31, 0.257]
Plan curvature	DEM	8.9 m	[2.44, 14.91, 0.775]; (14.91, 20.43, 0.899]; (20.43, 25.41, 1.221]; (25.41, 30.4, 1.064]; (30.4, 35.79, 1.123]; (35.79, 42.1, 1.033]; (42.1, 50.66, 0.895]; (50.66, 80.59, 0.578]
Relief amplitude	DEM	8.9 m	[1.21, 13.21, 1.676]; (31.21, 51.22, 2.07]; (51.22, 67.47, 1.101]; (67.47, 83.72, 0.845]; (83.72, 99.9, 0.712]; (99.9, 119.9, 0.589]; (119.9, 142.4, 0.368]; (142.4, 320.0, 0.06]
Lithology	National map	1:100,000	[hard clumpy intrusion rock (Y2), 0.493]; [limestone and dolomite rock (T1), 0.985]; [slate and phyllite (B1), 0.707]; [schist (T2), 0.607]; [sandstone, glutenite and mudstone (S2), 1.142]; [coal sandstone, shale and mudstone (S4), 1.083]; [sandstone and shale (S5), 1.274]; [water, 0]
TWI	DEM	8.9 m	[3.21, 4.80, 0.336]; (4.80, 5.29, 0.527]; (5.29, 5.78, 1.027]; (5.78, 6.26, 1.171]; (6.26, 7.00, 1.549]; (7.00, 7.85, 1.481]; (7.85, 8.83, 2.213]; (8.83, 34.38, 1.362]
NDBI	Landsat TM 8 images	1:25,000	[0.1, 0.28, 0.203]; (0.28, 0.35, 0.413]; (0.35, 0.40, 0.614]; (0.40, 0.46, 0.894]; (0.46, 0.52, 1.429]; (0.52, 0.61, 1.975]; (0.61, 0.75, 2.306]; (0.75, 1, 1.875]
NDVI	Landsat TM 8 images	1:25,000	[0, 0.14, 0.512]; (0.14, 0.23, 1.337]; (0.23, 0.28, 1.911]; (0.28, 0.31, 1.554]; (0.31, 0.33, 1.104]; (0.33, 0.36, 0.82]; (0.36, 0.39, 0.519]; (0.39, 0.48, 0.142]
River density (km/km^2)	DEM	8.9 m	[0, 0.43, 0.157]; (0.43, 0.63, 0.346]; (0.63, 0.80, 0.76]; (0.80, 0.96, 1.183]; (0.96, 1.11, 1.041]; (1.11, 1.28, 1.22]; (1.28, 1.47, 1.561]; (1.47, 1.95, 1.687]
Road density (km/km^2)	Google Earth	1:25,000	[0, 1.37, 0.432]; (1.37, 1.83, 1.36]; (1.83, 2.29, 1.941]; (2.29, 2.78, 2.646]; (2.78, 3.32, 3.158]; (3.32, 3.94, 3.026]; (3.94, 4.75, 3.1]; (4.75, 6.89, 2.176]

Note: In [a, b, c], a and b represent the lower and upper limit value for each conditioning factor class; c represents the FR value.

labeled value of 1 and non-landslide data with a labeled value of 0. The balance of landslide (positive) and non-landslide (negative) samples plays a crucial role in the process of LSP using machine learning models, which is still an important issue to be deeply studied. Some research has been carried out on this issue and some satisfactory results have been revealed (Hong et al., 2019; Pourghasemi et al., 2020; Yang et al., 2022). However, owing to the differences in the study area, machine learning models, mapping unit selection, landslide features and other factors, the conclusions of previous studies are different and it is difficult to obtain the optimal ratio. Hence, the ratio between landslide and non-landslide samples is set at 1:1 in this study, which is the most widely used ratio (Huang et al., 2021b).

In this study, 244 landslide slope units are totally included where landslides had occurred, which are labeled 1. The same number of non-landslide slope units, which are randomly sampled from the landslide-free area, are labeled 0. The landslide and non-landslide slope units are combinate as training samples, and then the slope unit-based conditioning factors FR values in Table 1 of training samples have been extracted as the input data to develop SVM models. Afterwards, training samples are randomly spilt into a training dataset and a testing dataset with a ratio of 70%/30% to develop the SVM model and to validate the predicting performance. For the slope unit-based SVM model, the radial basis function is selected as the kernel function, the optimum values of C and Gamma are assigned to be 5 and 1 based on the ten-fold cross-testing method. Hence, the landslide susceptibility indexes of all slope units in the study area can be predicted by the SVM model. Then, the Euclidean distance between landslide points and slope unit points and NSDI values can be calculated to develop the SVM-NSDI model. Finally, the SVM-updating model can be developed to update the LSP values by adding the LSP variation and the LSP values of SVM-NSDI model.

4. Results

4.1. Determination of distance threshold

To determine the optimal distance threshold between landslides and slope units with very high landslide susceptibility level, several different distance threshold values of 1000, 1500, 2000, 2100, 2500, 3000, 4000, 5000, 6000, 7000, 8000 and 9000 m are used to calculate the Euclidean distance between the central points of landslides and slope units. If the distance threshold is too short, more slope units with very high level won't be selected. On the contrary, if the distance threshold is too long, more slope units with very high level will be excessively considered. Hence, the optimal distance threshold is determined by analyzing the numbers of slope units with very high levels and landslides for each distance threshold. It can be seen from Fig. 6 that the quantity of slope units with very high levels and the quantity of landslides within each distance threshold tend to increase and then stabilize along with the increase in distance threshold value. When the distance threshold value is equal to 3000, all landslides in this study and 93.5% of slope units with very high level are included for analysis. Therefore, 3000 m is determined as the final optimal distance threshold.

4.2. Landslide susceptibility mappings of SVM, SVM-NSDI and SVM-Updating models

Based on the SVM, SVM-NSDI and SVM-Updating models, the LSP result for each model can be predicted and divided into five levels (very high, high, moderate, low and very low) using the natural break point method in ArcGIS 10.2 software. The landslide susceptibility mappings are shown in Fig. 7. The very high, high,

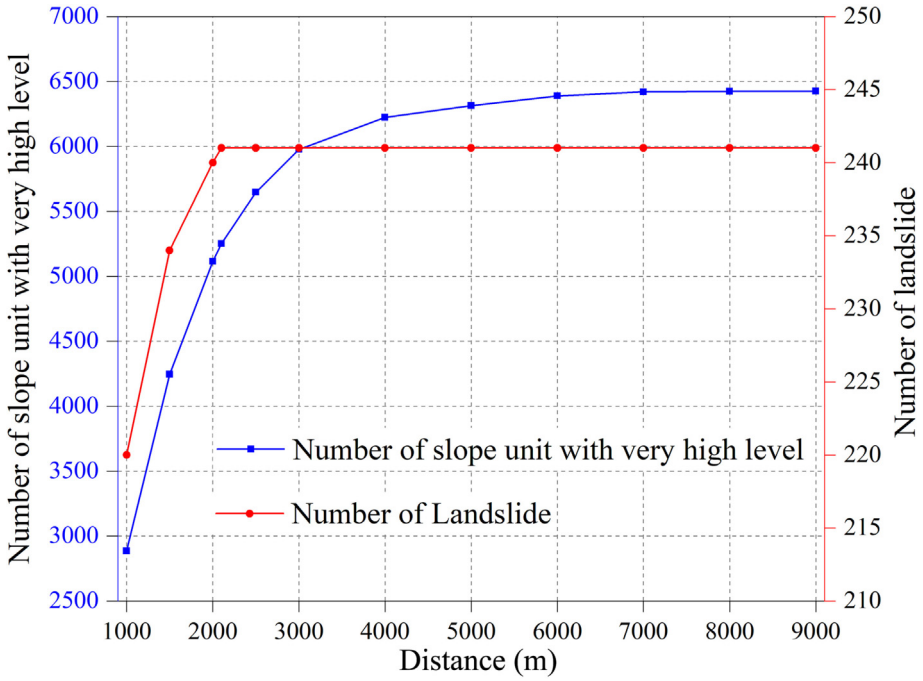

Fig. 6. The number of slope units with very high levels and landslides for different distance threshold.

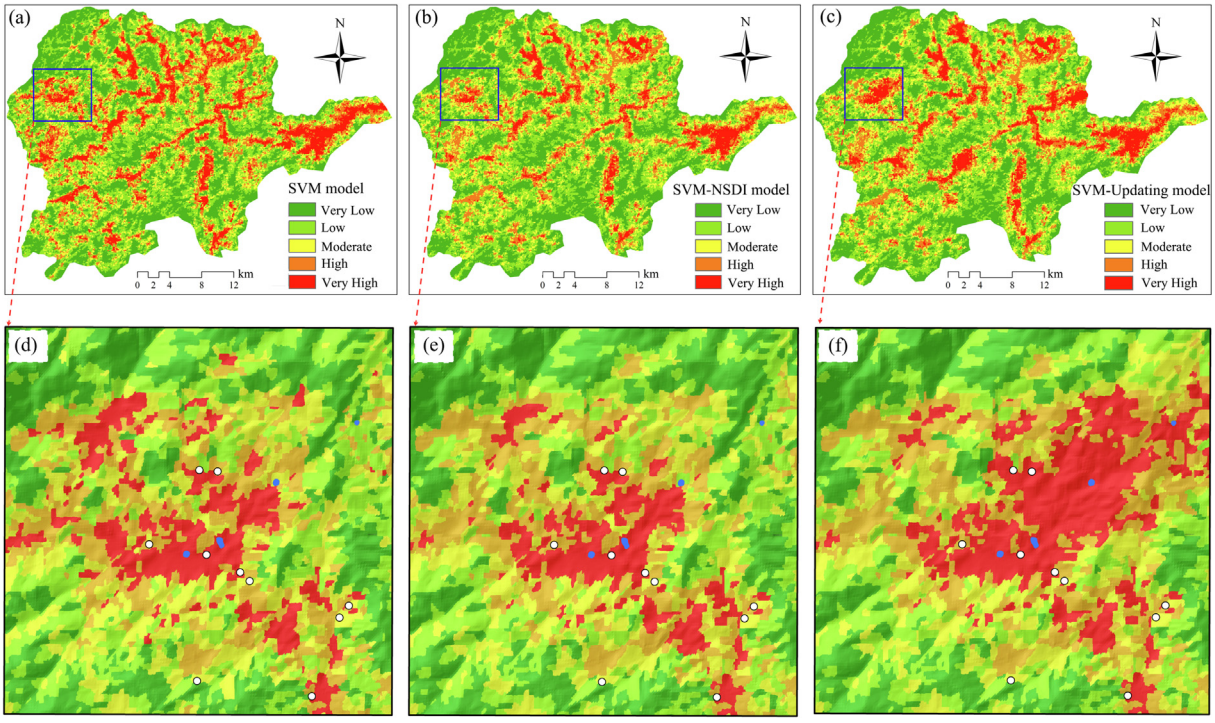

Fig. 7. Landslide susceptibility mappings of SVM, SVM-NSDI and SVM-Updating models (the white and blue points represent the old landslides and fresh landslides).

moderate, low and very low level account for 12.1%, 14.6%, 18.2%, 28.0% and 27.2% (Fig. 7a) for SVM model, 6.8%, 13.9%, 18.9%, 30.0% and 30.3% (Fig. 7b) for SVM-NSDI model, and 9.4%, 14.8%, 19.2%, 29.1% and 27.5% for SVM-Updating model (Fig. 7c). To clearly indicate and compare the differences of above landslide susceptibility mappings, a certain same zone (blue rectangle zone) has been enlarged and shown in Fig. 7d–f. Comparing the landslide susceptibility mappings of SVM and SVM-NSDI models, it can be found that the percentage of very high and high levels significantly decreases and the spatial distribution extracts a certain band. For the landslide susceptibility mapping of the SVM-Updating model, the spatial distribution of very high and high levels shows the feature of block-shaped around the fresh landslides.

4.3. Landslide susceptibility index distribution of SVM, SVM-NSDI and SVM-Updating models

The differences between different LSP models can be represented and compared by analyzing the landslide susceptibility index distribution. The mean and standard deviation values of landslide susceptibility indexes are two important indicators to reflect the mean level and dispersion degree of the landslide susceptibility index distribution. It is known that the lower the mean value is, the more landslide susceptibility indexes are primarily concentrated in the low and very low landslide susceptibility levels. The larger the standard deviation value is, the higher the dispersion is. The landslide susceptibility index distribution of SVM, SVM-NSDI and SVM-Updating models is shown in Fig. 8. The distribution patterns of landslide susceptibility indexes for SVM, SVM-NSDI and SVM-Updating models conform to a logarithmic normal distribution (red line). The mean values of landslide susceptibility indexes for SVM, SVM-NSDI and SVM-Updating models are 0.399, 0.436 and 0.461, respectively, with an increasing tendency. Similarly, the standard deviations of landslide susceptibility indexes exhibit the same tendency. It can be concluded that when the spatial correlation between landslides and slope units are considered and the landslide susceptibility indexes of slope units are updated by fresh landslides, the landslide susceptibility indexes of all slope units exhibit an increasing tendency.

4.4. Accuracy assessment and validation

4.4.1. Confusion-matrix-based statistical indices

In this study, based on the confusion matrix of LSP models, the accuracy, precision, recall and F_1-score are calculated and shown in Table 2. It is revealed that the accuracy values of SVM, SVM-NSDI and SVM-Updating models are 0.793, 0.817 and 0.819, respectively. F_1-score values of SVM, SVM-NSDI and SVM-Updating models are 0.776, 0.816 and 0.831, respectively, indicating that the SVM-NSDI model that considering the spatial correlation between landslides and slope units has a better prediction performance than that of the SVM model. The LSP results of SVM-Updating model based on the fresh landslides information also have greater prediction performance than that of the SVM and SVM-NSDI models.

4.4.2. ROC curve

The ROC curve is the most effective and widely used method to evaluate the prediction performance of LSP models. The AUC value (under the area of ROC curve) can be used to quantitatively compare the prediction performance of the different LSP models. The ROC curves of LSP models in this study are shown in Fig. 9. The AUC values of SVM, SVM-NSDI and SVM-Updating models are 0.869, 0.903 and 0.914, respectively. It can be concluded that the prediction performances of the SVM-NSDI and SVM-Updating models are better than that of the SVM model, indicating that the LSP results are more scientific when the spatial correlation between landslides and slope units are taken into account. Furthermore, the LSP results can be updated based on the fresh landslide information.

4.4.3. FR accuracy

In this study, the FR accuracies of the SVM, SVM-NSDI and SVM-Updating models are shown in Table 3. The FR accuracies of the SVM, SVM-NSDI and SVM-Updating models are 0.795, 0.853 and 0.873, respectively, indicating that the prediction performance of SVM-NSDI model has a significant improvement than SVM model. Compared to the results of SVM-NSDI model, more landslides are located into very high, high levels and the LSP results can be updated with a satisfactory prediction performance.

5. Discussion

5.1. Variation of landslide susceptibility level in study area A

To illustrate the practicability and effectiveness, the study area A in Fig. 4 is taken as an example. In this study area, there are 3324 slope units, 19 pre-landslides and 6 fresh-landslides (Fig. 10). The landslide susceptibility results of SVM, SVM-NSDI and SVM-Updating models in area A are shown in Fig. 11. Based on the LSP results of the SVM model, there are a total of 504 slope units with very high level and 538 slope units with high level. It can be found that those slope units are mainly distributed along the highway and construction area. When considering the spatial correlation between landslides and slope units, the number of slope units with very high and high levels is 277 and 527, respectively. Moreover, the LSP results are updated based on six fresh-landslides. There are 517 slope units with very high level and 659 slope units with high level. It is revealed that more information and effects on adjacent slope units of those fresh landslides can be integrated into LSP results when the LSP results are updated.

5.2. The comparison of LSP performance for SVM, SVM-NSDI and SVM-Updating models

In this study, the prediction performances of SVM, SVM-NSDI and SVM-Updating models are evaluated using confusion matrix-based statistical indices, ROC curve and FR accuracy method. The SVM-NSDI model has better prediction performance compared with that of the SVM model, indicating that the spatial correlation between landslides and mapping units needs to be taken into account during the LSP process. This is because the same types of landslides are prone to occur under the same inducing conditioning factors. In particular, for the rainfall-trigging shallow landslide, the spatial distribution of this type landslide demonstrates the feature of spatial aggregation at a certain scale, which is similar to

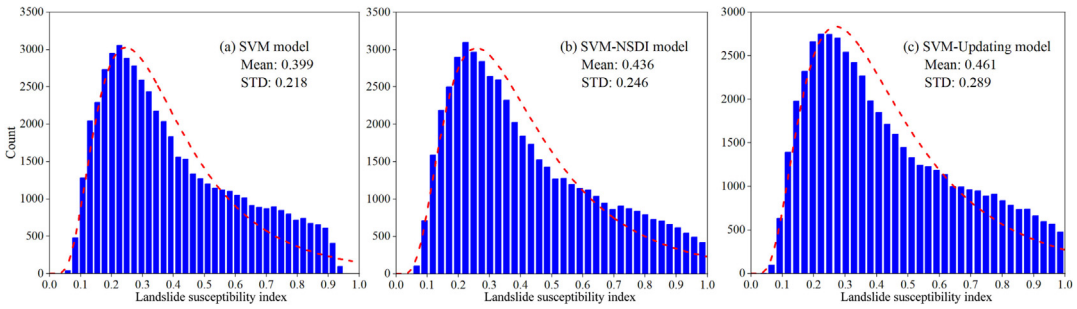

Fig. 8. Landslide susceptibility index distribution features of SVM, SVM-NSDI and SVM-Updating models (STD: standard deviation).

Table 2
The accuracy, precision, recall and F_1-score indicators for different LSP models.

Model	TP	FP	FN	TN	Accuracy	Precision	Recall	F_1-score
SVM	173	32	68	209	0.793	0.844	0.718	0.776
SVM-NDSI	195	42	46	199	0.817	0.823	0.809	0.816
SVM-Updating	226	50	42	191	0.819	0.819	0.843	0.831

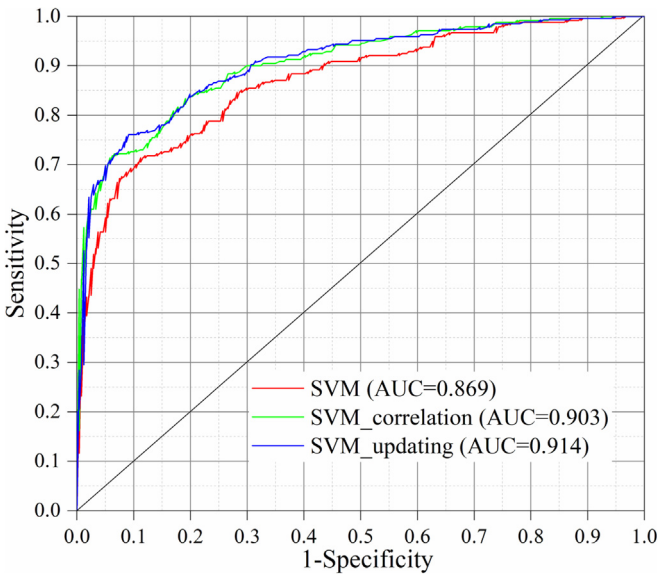

Fig. 9. ROC curves of SVM, SVM-NSDI and SVM-Updating models.

that related to natural clustering (Li et al., 2011; Wang et al., 2013; Liu et al., 2019). On the other hand, the prediction performance results reveal that the SVM-Updating model has better performance than that of the SVM and SVM-NSDI models. Due to the abundant engineering construction and extreme climate conditions recently, the landform is undergoing drastic changes, resulting in some differences in conditioning factors between pre- and fresh-landslides (Lin and Wang, 2018; Rosi et al., 2018). In the SVM-Updating model, more information about fresh landslides can be incorporated into LSP model to improve the accuracy of LSP results.

5.3. Evaluation of the proposed method

In the precious literature of landslide susceptibility (Lombardo et al., 2020; Liu et al., 2023), there are two main limitations in LSP process on the spatial and temporal scales. One of the limitations is that the spatial correlation between landslides and mapping units has not been explicitly considered. This means that the adjacent and distant mapping units around landslides are equally taken into account by the LSP models, which may cause a large bias for the predictive performance (Goetz et al., 2015; Lombardo et al., 2018). The other limitation is that the LSP results in an area are stationary in time. This is not valid because the conditioning factors inducing landslides (such as rainfall and land cover) may change over a period of time. In addition, the landslide inventory also needs to be updated along with the occurrence of fresh landslides. Focusing on above limitations in this study, landslide susceptibility has been predicted and updated considering the spatial and temporal effects of landslide. The spatial correlations between landslides and slope units have been represented by the NSDI indicator, which can quantitatively characterize the effect of landslides on their surrounding slope units, along with higher predicted performance for LSP models. Furthermore, the SVM-Updating model has been developed to update the LSP results using fresh landslides. It is revealed that the LSP updating results have higher accuracy and the spatial and temporal effects of landslide have been successfully implemented in LSP.

Moreover, compared with the previous landslide susceptibility updating methods (Guzzetti et al., 2012; Samia et al., 2018; Depina et al., 2020), the main advantage of this study is that the spatial and temporal effects of landslide can be taken into account simultaneously in LSP at the regional scale. Especially for the study area that without complete high-resolution multi-temporal landslide inventory, the effect of fresh landslides on surrounding slope units within a certain distance can be fully represented to update landslide susceptibility. In addition, the method of this study has stronger applicability at a larger scale and doesn't need to collect detailed geotechnical and hydrological data compared with physically-based models. However, there are still some drawbacks that need to be improved. For example, the differences between the slope unit that are affected by landslide and adjacent slope units (such as aspect) have not been considered. The application of this method at different scales needs to be further studied. Moreover, the landslide inventory is just divided into pre- and

Table 3
FR accuracy of different LSP models.

Model	LSL	Threshold value	Proportion of slope unit	Proportion of landslide	FR	Accuracy
SVM model	Very High	(0.71, 1]	0.121	0.466	3.851	0.795
	High	(0.53, 0.71]	0.146	0.231	1.590	
	Moderate	(0.37, 0.53]	0.182	0.168	0.924	
	Low	(0.23, 0.37]	0.280	0.101	0.360	
	Very Low	[0.0, 0.23]	0.272	0.034	0.124	
SVM-NDSI	Very High	(0.89, 1]	0.068	0.392	5.737	0.853
	High	(0.65, 0.89]	0.139	0.295	2.113	
	Moderate	(0.44, 0.65]	0.189	0.160	0.849	
	Low	(0.26, 0.44]	0.300	0.123	0.410	
	Very Low	[0.0, 0.26]	0.303	0.030	0.099	
SVM-Updating	Very High	(0.89, 1]	0.094	0.520	5.532	0.873
	High	(0.65, 0.89]	0.148	0.243	1.642	
	Moderate	(0.44, 0.65]	0.192	0.124	0.646	
	Low	(0.26, 0.44]	0.291	0.087	0.299	
	Very Low	[0.0, 0.26]	0.275	0.026	0.095	

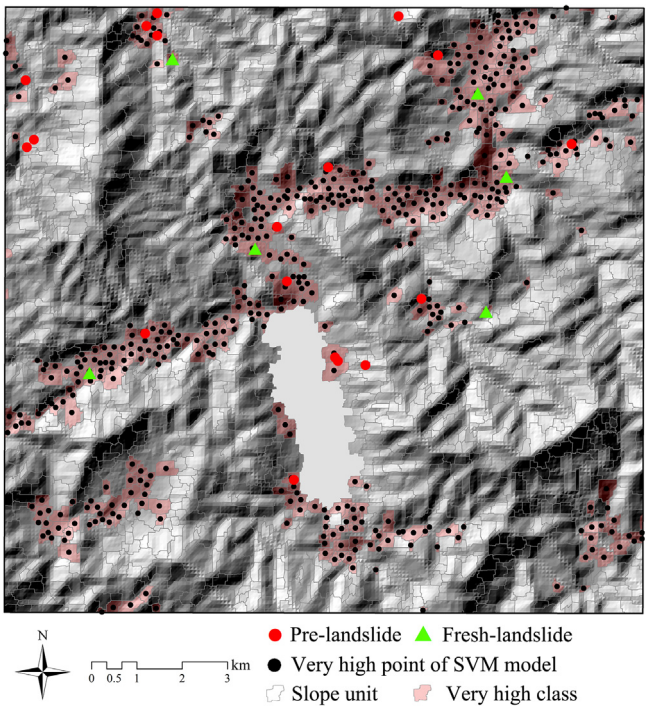

Fig. 10. The distribution of slope units with very high levels and landslides in study area A.

fresh-landslide inventories due to the limited landslide data in this study.

6. Conclusion

In this study, the spatial correlation between slope units and landslides has been quantitatively represented, and landslide susceptibility has been updated by integrating the fresh landslide information with LSP results. Based on the LSP results of the SVM model, the SVM-NSDI and SVM-Updating models are constructed. Some novel and significant conclusions can be drawn:

(1) NSDI is an effective indicator to quantify the spatial correlation between landslides and slope units. The optimal distance threshold between landslides and slope units with very high level is determined as 3000 m in this study.
(2) The results of matrix confusion-based statistical indices, AUC and FR accuracy for SVM, SVM-NSDI and SVM-Updating models indicate that the prediction performance of the SVM-NSDI model is better than that of the SVM model. In addition, the prediction performance of the SVM-Updating model is better than that of the SVM and SVM-NSDI models. It can be concluded that the landslide susceptibility can be updated based on the spatial and temporal effect of landslides.

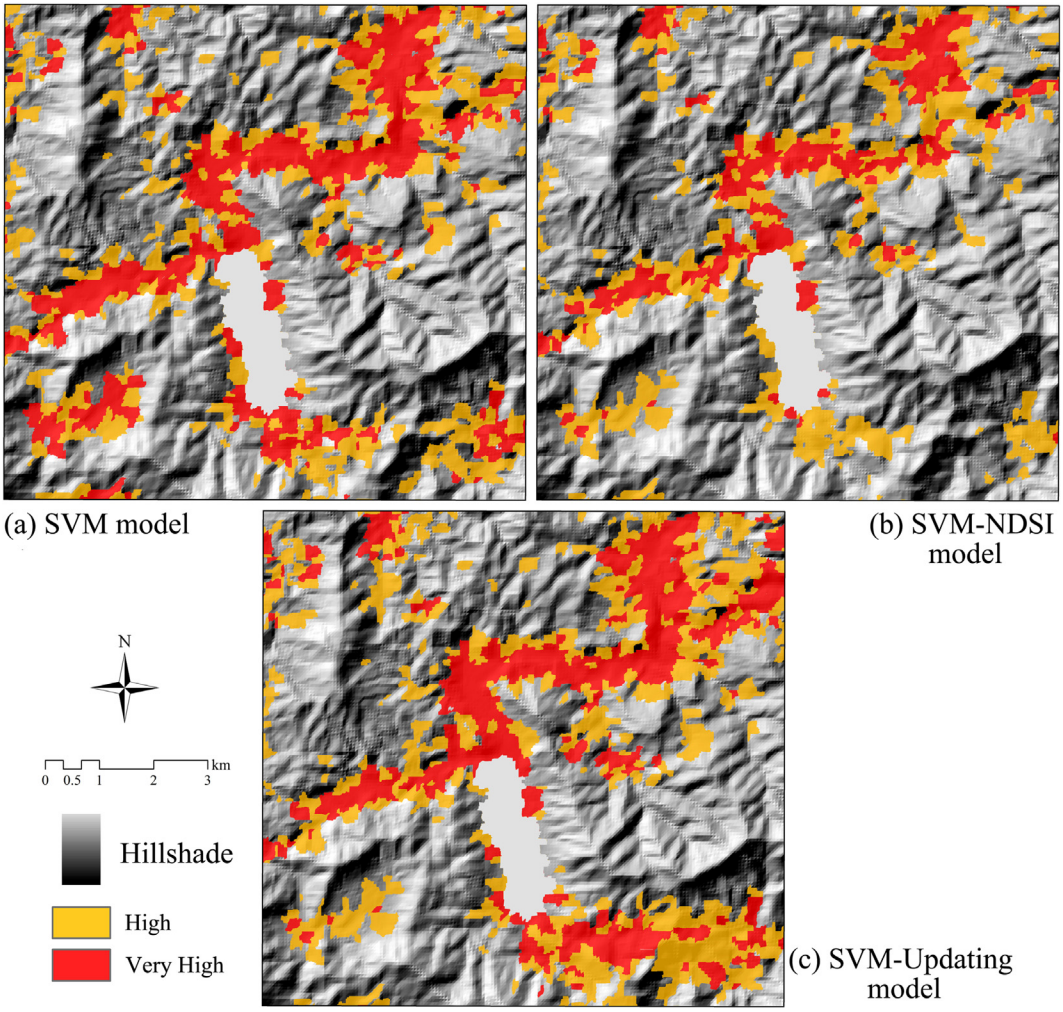

Fig. 11. Landslide susceptibility level in area A of SVM, SVM-NSDI and SVM-Updating models.

(3) It is revealed that the landslide susceptibility is a time-variant variable rather than a stationary variable, which can be updated based on the multi-temporal landslide inventory.

CRediT authorship contribution statement

Zhilu Chang: Methodology, Data curation, Software, Writing – original draft. **Faming Huang:** Conceptualization, Supervision, Writing – review & editing. **Jinsong Huang:** Conceptualization, Supervision, Writing – review & editing. **Shui-Hua Jiang:** Conceptualization, Supervision, Writing – review & editing. **Yuting Liu:** Writing – review & editing. **Sansar Raj Meena:** Visualization, Writing – review & editing. **Filippo Catani:** Supervision, Validation, Writing – review & editing.

Declaration of Competing Interest

The authors declare that they have no known competing financial interests or personal relationships that could have appeared to influence the work reported in this paper.

Acknowledgements

This research is funded by the National Natural Science Foundation of China (Nos. 52222905, 52179103, 41807285, 41972280 and 42272326), China Postdoctoral Science Foundation (No. 2019M652287), Jiangxi Provincial Natural Science Foundation (Nos. 20181ACB20008, 20192BBG70078). The first author would like to thank the China Scholarship Council for funding his research at the University of Padua, Italy.

References

Al-Najjar, H.A.H., Pradhan, B., 2021. Spatial landslide susceptibility assessment using machine learning techniques assisted by additional data created with generative adversarial networks. Geosci. Front. 12, 625–637. https://doi.org/10.1016/j.gsf.2020.09.002.

Chang, Z., Du, Z., Zhang, F., Huang, F., Chen, J., Li, W., Guo, Z., 2020. Landslide susceptibility prediction based on remote sensing images and GIS: Comparisons of supervised and unsupervised machine learning models. Remote Sens. 12 (3), 502. https://doi.org/10.3390/rs12030502.

Chang, Z., Huang, J., Huang, F., Bhuyan, K., Meena, S.R., Catani, F., 2023. Uncertainty analysis of non-landslide sample selection in landslide susceptibility prediction using slope unit-based machine learning models. Gondwana Res. 117, 307–320. https://doi.org/10.1016/j.gr.2023.02.007.

Del Ventisette, C., Righini, G., Moretti, S., Casagli, N., 2014. Multitemporal landslides inventory map updating using spaceborne SAR analysis. Int. J. Appl. Earth Obs. Geoinf. 30, 238–246. https://doi.org/10.1016/j.jag.2014.02.008.

Depina, I., Oguz, E.A., Thakur, V., 2020. Novel Bayesian framework for calibration of spatially distributed physical-based landslide prediction models. Comput. Geotech. 125, 103660. https://doi.org/10.1016/j.compgeo.2020.103660.

Fan, L., Lehmann, P., Or, D., 2015. Effects of hydromechanical loading history and antecedent soil mechanical damage on shallow landslide triggering. J. Geophys. Res.: Earth Surface 120 (10), 1990–2015. https://doi.org/10.1002/2015JF003615.

Goetz, J.N., Brenning, A., Petschko, H., Leopold, P., 2015. Evaluating machine learning and statistical prediction techniques for landslide susceptibility modeling. Comput. Geosci. 81, 1–11. https://doi.org/10.1016/j.cageo.2015.04.007.

Gojcic, Z., Schmid, L., Wieser, A., 2021. Dense 3D displacement vector fields for point cloud-based landslide monitoring. Landslides 18, 3821–3832. https://doi.org/10.1007/s10346-021-01761-y.

Guzzetti, F., Carrara, A., Cardinali, M., Reichenbach, P., 1999. Landslide hazard evaluation: a review of current techniques and their application in a multi-scale study, Central Italy. Geomorphology 31, 181–216.

Guzzetti, F., Reichenbach, P., Cardinali, M., Galli, M., Ardizzone, F., 2005. Probabilistic landslide hazard assessment at the basin scale. Geomorphology 72, 272–299. https://doi.org/10.1016/j.geomorph.2005.06.002.

Guzzetti, F., Mondini, A.C., Cardinali, M., Fiorucci, F., Santangelo, M., Chang, K.-T., 2012. Landslide inventory maps: New tools for an old problem. Earth-Sci. Rev. 112, 42–66. https://doi.org/10.1016/j.earscirev.2012.02.001.

Hong, H., Miao, Y., Liu, J., Zhu, A.X., 2019. Exploring the effects of the design and quantity of absence data on the performance of random forest-based landslide susceptibility mapping. Catena 176, 45–64. https://doi.org/10.1016/j.catena.2018.12.035.

Huabin, W., Gangjun, L., Weiya, X., Gonghui, W., 2016. GIS-based landslide hazard assessment: an overview. Prog. Phys. Geog.: Earth Environ. 29, 548–567. https://doi.org/10.1191/0309133305 pp462ra.

Huang, F., Tao, S., Chang, Z., Huang, J., Fan, X., Jiang, S.H., Li, W., 2021a. Efficient and automatic extraction of slope units based on multi-scale segmentation method for landslide assessments. Landslides 18 (11), 3715–3731. https://doi.org/10.1007/s10346-021-01756-9.

Huang, F., Ye, Z., Jiang, S.-H., Huang, J., Chang, Z., Chen, J., 2021b. Uncertainty study of landslide susceptibility prediction considering the different attribute interval numbers of environmental factors and different data-based models. Catena 202, 105250. https://doi.org/10.1016/j.catena.2021.105250.

Huang, F., Yan, J., Fan, X., Yao, C., Huang, J., Chen, W., Hong, H., 2022. Uncertainty pattern in landslide susceptibility prediction modelling: Effects of different landslide boundaries and spatial shape expressions. Geosci. Front. 13 (2), 101317. https://doi.org/10.1016/j.gsf.2021.101317.

Ji, J., Cui, H., Zhang, T., Song, J., Gao, Y., 2022. A GIS-based tool for probabilistic physical modelling and prediction of landslides: GIS-FORM landslide susceptibility analysis in seismic areas. Landslides 19, 2213–2231. https://doi.org/10.1007/s10346-022-01885-9.

Jiang, S.-H., Huang, J., Huang, F., Yang, J., Yao, C., Zhou, C.-B., 2018. Modelling of spatial variability of soil undrained shear strength by conditional random fields for slope reliability analysis. Appl. Math. Modell. 63, 374–389. https://doi.org/10.1016/j.apm.2018.06.030.

Li, C., Ma, T., Sun, L., Li, W., Zheng, A., 2011. Application and verification of a fractal approach to landslide susceptibility mapping. Nat. Hazards 61, 169–185. https://doi.org/10.1007/s11069-011-9804-x.

Lin, Q., Wang, Y., 2018. Spatial and temporal analysis of a fatal landslide inventory in China from 1950 to 2016. Landslides 15, 2357–2372. https://doi.org/10.1007/s10346-018-1037-6.

Liu, S., Wang, L., Zhang, W., He, Y., Samui, P., 2023. A comprehensive review of machine learning-based methods in landslide susceptibility mapping. Geol. J., in press. https://doi.org/10.1002/gj.4666.

Liu, L., Li, S., Li, X., Jiang, Y., Wei, W., Wang, Z., Bai, Y., 2019. An integrated approach for landslide susceptibility mapping by considering spatial correlation and fractal distribution of clustered landslide data. Landslides 16, 715–728. https://doi.org/10.1007/s10346-018-01122-2.

Lombardo, L., Opitz, T., Huser, R., 2018. Point process-based modeling of multiple debris flow landslides using INLA: an application to the 2009 Messina disaster. Stoch. Environ. Res. Risk Assess. 32, 2179–2198. https://doi.org/10.1007/s00477-018-1518-0.

Lombardo, L., Opitz, T., Ardizzone, F., Guzzetti, F., Huser, R., 2020. Space-time landslide predictive modelling. Earth-Sci. Rev. 209, 103318. https://doi.org/10.1016/j.earscirev.2020.103318.

Merghadi, A., Yunus, A.P., Dou, J., Whiteley, J., ThaiPham, B., Bui, D.T., Avtar, R., Abderrahmane, B., 2020. Machine learning methods for landslide susceptibility studies: A comparative overview of algorithm performance. Earth-Sci. Rev. 207, 103225. https://doi.org/10.1016/j.earscirev.2020.103225.

Ng, C.W.W., Yang, B., Liu, Z.Q., Kwan, J.S.H., Chen, L., 2021. Spatiotemporal modelling of rainfall-induced landslides using machine learning. Landslides 18, 2499–2514. https://doi.org/10.1007/s10346-021-01662-0.

Parker, R., Hancox, G., Petley, D., Massey, C., Densmore, A., Rosser, N., 2015. Spatial distributions of earthquake-induced landslides and hillevelope preconditioning in the northwest South Island, New Zealand. Earth Surf. Dyn. 3 (4), 501–525. https://doi.org/10.5194/esurf-3-501-2015.

Phillips, J.D., 2006. Evolutionary geomorphology: thresholds and nonlinearity in landform response to environmental change. Hydrol. Earth Syst. Sci. 10 (5), 731–742. https://doi.org/10.5194/hess-10-731-2006.

Pourghasemi, H.R., Kornejady, A., Kerle, N., Shabani, F., 2020. Investigating the effects of different landslide positioning techniques, landslide partitioning approaches, and presence-absence balances on landslide susceptibility mapping. Catena 187, 104364. https://doi.org/10.1016/j.catena.2019.104364.

Reichenbach, P., Rossi, M., Malamud, B.D., Mihir, M., Guzzetti, F., 2018. A review of statistically-based landslide susceptibility models. Earth-Sci. Rev. 180, 60–91. https://doi.org/10.1016/j.earscirev.2018.03.001.

Rosi, A., Tofani, V., Tanteri, L., Tacconi Stefanelli, C., Agostini, A., Catani, F., Casagli, N., 2018. The new landslide inventory of Tuscany (Italy) updated with PS-InSAR: geomorphological features and landslide distribution. Landslides 15, 5–19. https://doi.org/10.1007/s10346-017-0861-4.

Samia, J., Temme, A., Bregt, A., Wallinga, J., Guzzetti, F., Ardizzone, F., Rossi, M., 2017a. Do landslides follow landslides? Insights in path dependency from a multi-temporal landslide inventory. Landslides 14, 547–558. https://doi.org/10.1007/s10346-016-0739-x.

Samia, J., Temme, A., Bregt, A., Wallinga, J., Guzzetti, F., Ardizzone, F., Rossi, M., 2017b. Characterization and quantification of path dependency in landslide susceptibility. Geomorphology 292, 16–24. https://doi.org/10.1016/j.geomorph.2017.04.039.

Samia, J., Temme, A.J.A.M., Bregt, A.K., Wallinga, J., Stuiver, J., Guzzetti, F., Ardizzone, F., Rossi, M., 2018. Implementing landslide path dependency in landslide susceptibility modelling. Landslides 15, 2129–2144. https://doi.org/10.1007/s10346-018-1024-y.

Samia, J., Temme, A., Bregt, A., Wallinga, J., Guzzetti, F., Ardizzone, F., 2020. Dynamic path-dependent landslide susceptibility modelling. Nat. Hazards Earth Syst. Sci. 20, 271–285. https://doi.org/10.5194/nhess-20-271-2020.

Singh, K., Mehrotra, A., Pal, K., 2014. Landslide detection from satellite images using spectral indices and digital elevation model. Disaster Adv. 7 (6), 25–32.
Sun, D., Gu, Q., Wen, H., Shi, S., Mi, C., Zhang, F., 2022. A hybrid landslide warning model coupling susceptibility zoning and precipitation. Forests 13 (6), 827. https://doi.org/10.3390/f13060827.
Temme, A.J.A.M., Keiler, M., Karssenberg, D., Lang, A., 2015. Complexity and non-linearity in earth surface processes - concepts, methods and applications. Earth Surf. Processes Landforms 40, 1270–1274. https://doi.org/10.1002/esp.3712.
Tseng, C.M., Lin, C.W., Hsieh, W.D., 2015. Landslide susceptibility analysis by means of event-based multi-temporal landslide inventories. Nat. Hazards Earth Syst. Sci. 3 (2), 1137–1173. https://doi.org/10.5194/nhessd-3-1137-2015.
Wang, Y., Huang, J., Tang, H., Zeng, C., 2020. Bayesian back analysis of landslides considering slip surface uncertainty. Landslides 17, 2125-2136. https://doi.org/10.1007/s10346-020-01432-4.
Wang, H.J., Xiao, T., Li, X.Y., Zhang, L.L., Zhang, L.M., 2019. A novel physically-based model for updating landslide susceptibility. Eng. Geol. 251, 71–80. https://doi.org/10.1016/j.enggeo.2019.02.004.
Wang, X., Zhang, L., Wang, S., Lari, S., 2013. Regional landslide susceptibility zoning with considering the aggregation of landslide points and the weights of factors. Landslides 11, 399–409. https://doi.org/10.1007/s10346-013-0392-6.
Wang, H., Zhang, L., Yin, K., Luo, H., Li, J., 2021. Landslide identification using machine learning. Geosci. Front. 12, 351–364. https://doi.org/10.1016/j.gsf.2020.02.012.
Yang, C., Liu, L.-L., Huang, F., Huang, L., Wang, X.-M., 2022. Machine learning-based landslide susceptibility assessment with optimized ratio of landslide to non-landslide samples. Gondwana Res., in press. https://doi.org/10.1016/j.gr.2022.05.012.
Yong, C., Jinlong, D., Fei, G., Bin, T., Tao, Z., Hao, F., Li, W., Qinghua, Z., 2022. Review of landslide susceptibility assessment based on knowledge mapping. Stoch. Environ. Res. Risk Assess. 36, 2399–2417. https://doi.org/10.1007/s00477-021-02165-z.
Youssef, A.M., Pourghasemi, H.R., Pourtaghi, Z.S., Al-Katheeri, M.M., 2015. Landslide susceptibility mapping using random forest, boosted regression tree, classification and regression tree, and general linear models and comparison of their performance at Wadi Tayyah Basin, Asir Region, Saudi Arabia. Landslides 13, 839–856. https://doi.org/10.1007/s10346-015-0614-1.
Zhang, W.G., He, Y.W., Wang, L.Q., Liu, S.L., Meng, X.Y., 2023. Landslide susceptibility mapping using random forest and extreme gradient boosting: A case study of Fengjie, Chongqing. Geol. J., in press. https://doi.org/10.1002/gj.4683.
Zhou, X., Wen, H., Zhang, Y., Xu, J., Zhang, W., 2021. Landslide susceptibility mapping using hybrid random forest with GeoDetector and RFE for factor optimization. Geosci. Front. 12 (5), 101211. https://doi.org/10.1016/j.gsf.2021.101211.
Zhou, X., Wen, H., Li, Z., Zhang, H., Zhang, W., 2022. An interpretable model for the susceptibility of rainfall-induced shallow landslides based on SHAP and XGBoost. Geocart. Internat. 1–32. https://doi.org/10.1080/10106049.2022.2076928.